Supporting Information

Abelein et al. 10.1073/pnas.1421961112

Sample Preparation

Recombinant $A\beta_{40}$ peptide was purchased from Alexo-Tech and samples were prepared as in ref. 1. Experiments were performed in 10 mM Hepes buffer, pH 7.4, in 10 or 100% D_2O (for diffusion experiments) for NMR and 10 mM sodium-phosphate buffer, pH 7.2–7.4, with 0.02% NaN_3 for kinetics experiments, respectively. Zn^{2+} ions were added using $ZnCl_2$ stock solutions.

Aggregation Kinetics

Experimental Setup. ThT fluorescence aggregation kinetics were measured using a 96-well plate on a Fluostar Omega (BMG Labtech) fluorometer. ThT was diluted from a 4 mM ThT stock solution to a final concentration of 40 μM (unseeded experiments) or 100 μM (preseeded experiments). Experiments were performed at 37 °C under quiescent conditions and the signals were recorded in an interval time of 300 s for unseeded and 60 or 20 s for preseeded experiments. All peptide samples were prepared and kept on ice and quickly transferred to the 96-well plate just before measuring.

Analysis. Kinetic traces at different peptide concentrations with and without Zn^{2+} in $A\beta_{40}$:Zn^{2+} 10:1 molar equivalents were primarily fitted to sigmoidal functions that can be described by $F = F_0 + A/(1 + \exp[r_{max}(\tau_{1/2} - t)])$, where $\tau_{1/2}$ is the time for depletion of half of the monomer pool by aggregation and r_{max} is the maximum growth rate. Averaged $\tau_{1/2}$ values (four or five replicates), which were weighted by their variances, show a dependence on the initial monomer concentration, $m(0)$, that is described by a power law $m(0)^{\gamma}$ where γ is the half-time exponent. Accordingly, kinetic traces (five replicates) of 20 μM $A\beta_{40}$ at different Zn^{2+} concentrations exhibit sigmoidal kinetic profiles whose averaged $\tau_{1/2}$ values show an exponential dependence on the Zn^{2+} concentration with $\tau_{1/2} = \tau_0 \cdot \exp([Zn^{2+}]/c_e)$.

In addition, a global fit analysis was performed including all aggregation kinetics data (see following sections).

Kinetic Model of Aggregation. We applied an aggregation kinetic model as proposed by Meisl et al. (2) that includes primary nucleation (k_n), elongation (k_+), and secondary nucleation (k_2) where the reaction orders n_c and n_2 describe primary and secondary nucleation events, respectively. In this model an equilibrium constant K_M is introduced to account for saturation of secondary nucleation following the terms of Michaelis–Menten kinetics (2). The primary and secondary reaction orders were set to $n_2 = n_c = 2$ as previously reported for $A\beta_{42}$ (3) and $A\beta_{40}$ (2). In addition, the choice of n_2 and n_c was validated by assigning one of them as an additional fitting parameter. These fits revealed values around 2 for n_2 and n_c or worse fits (larger χ^2 values) for other values. In this model, the normalized fraction of fibril mass, $M(t)/M(\infty)$, is described by

$$\frac{M(t)}{M(\infty)} = 1 - \left(\frac{B_+ + C_+}{B_+ + C_+ e^{\kappa t}} \frac{B_- + C_+ e^{\kappa t}}{B_- + C_+}\right)^{\frac{k_\infty^2}{\kappa \tilde{k}_\infty}} e^{-k_\infty t} \qquad [S1]$$

with global fit parameters that describe the formation of aggregates through primary nucleation,

$$\lambda = \sqrt{2k_+ k_n m(0)^{n_c}} \qquad [S2]$$

and secondary nucleation

$$\kappa = \sqrt{2k_+ k_2 \frac{m(0)^{n_2+1}}{1 + m(0)^{n_2}/K_M}}, \qquad [S3]$$

where $m(0)$ is the initial monomer concentration and K_M is the Michaelis constant.

The other parameters are related to λ and κ by

$$B_\pm = \left(k_\infty \pm \tilde{k}_\infty\right)/(2\kappa) \qquad [S4]$$

$$C_\pm = \pm\lambda^2/(2\kappa^2) \qquad [S5]$$

$$k_\infty = 2k_+ P(\infty) \qquad [S6]$$

$$\tilde{k}_\infty = \sqrt{k_\infty^2 - 2C_+ C_- \kappa^2}. \qquad [S7]$$

The long time limit of the aggregation number $P(\infty)$ for $n_2 = 2$ is given by (2)

$$2k_+ P(\infty) = \sqrt{|-A(0) - 2k_+ k_2 m(0) K_M \log(K_M)/n_2|} \qquad [S8]$$

with

$$A(0) = -\frac{2k_+ k_n m(0)^{n_c}}{n_c} - 2k_+ k_2 m(0) K_M \frac{\log(K_M + m(0)^{n_2})}{n_2} - 2k_+ k_2 K_M m(0)\left(\frac{\sqrt{K_M}\arctan\left(m(0)/\sqrt{K_M}\right)}{m(0)} - 1\right). \qquad [S9]$$

For a two-step secondary nucleation reaction the Michaelis constant K_M is defined by $K_M = (k_b + \bar{k}_2)/k_f$, which is related to k_2 by $k_2 = \bar{k}_2/K_M$. The rates k_f and k_b reflect the rate of attachment and detachment of n_2 monomers to/from the fibril surface, respectively, and $\bar{k}_2$ describes the subsequent release of the formed aggregate from the fibril surface.

Global fits were performed using all data from ThT fluorescence kinetics in an initial monomer concentration interval of 10–20 μM. Aggregation traces were normalized with respect to the initial and final fluorescence signals and averaged over four or five kinetic traces for each peptide concentration. Here, for each time point a variance weighted average was calculated. These normalized and variance weighted averaged kinetic traces were fitted globally using Eq. **S1** where global fit parameters were $\sqrt{k_+ k_n}$, $\sqrt{k_+ k_2}$ and $\sqrt{K_M}$ and the initial mass concentration was constrained to ±1 μM of the experimentally determined monomer concentration. In a second fit, to check the quality of the fit by reducing the number of free parameters, the value of $\sqrt{K_M}$ was held constant to the experimentally determined value, which led to the same fitting values but with a reduced fitting error.

Half-Time Exponent

The half-time exponent γ can be derived from Eq. **S1** and is given as (2)

$$\gamma = -0.5\left(\frac{n_2}{1 + m(0)^{n_2}/K_M} + 1\right). \qquad [S10]$$

With $n_2 = 2$ and an experimentally obtained half-time exponent of $\gamma = -0.91 \pm 0.12$ (Fig. 1*B*) the mean value for an initial monomer range of 10–20 μM is $\sqrt{K_M} = 12.5 \pm 1.5$ μM. This value was used in the global fit analysis for $A\beta_{40}$ aggregation at different Zn^{2+} concentrations (Fig. 2*A* and Fig. S4).

Attenuated Total Reflection Infrared

IR measurements were conducted at 4-cm^{-1} resolution using a Bruker Vertex 70 spectrometer equipped with a SensIR 9-reflection diamond attenuated total reflection (ATR) accessory. The samples were taken from ThT fluorescence measurements at the end state and after centrifugation for 20 min the precipitate was dried with a gentle nitrogen stream on the diamond crystal. Spectra were averaged over 10 scans and normalized to the intensity of the secondary derivative minimum at 1,625–1,629 cm^{-1}, which is a typical β-sheet feature (4). For $A\beta_{40}$ alone and in the presence of low zinc concentrations (≤2.5 μM) the spectra are almost identical, indicating a similar morphology of the fibril structures. In contrast, at 10 μM Zn^{2+} the IR spectrum is clearly different, suggesting the formation of different fibril morphologies under these conditions (Fig. S1).

Effect of Different Zn^{2+} Concentrations

To investigate the effect of Zn^{2+} on the microscopic rate constants a global fit analysis was performed using aggregation traces (average of five replicates per time point) of 20 μM $A\beta_{40}$ in the presence of 0–2.5 μM Zn^{2+}. Three different fits were performed where either k_n, k_+, or k_2 was effectively allowed to vary across different Zn^{2+} concentrations where, to reduce the numbers of freedom, $m(0)$ and $\sqrt{K_M}$ (set to 12.5 μM) were held constant. To investigate the effect on the secondary nucleation rate, k_2, the data were globally fitted to Eq. **S1** where $\sqrt{k_+k_n}$ was fixed to one global value for all Zn^{2+} concentrations whereas $\sqrt{k_+k_2}$ was allowed to vary between different concentrations. With this constraint, the secondary nucleation rate is the only effective free fitting parameter. In contrast, when holding $\sqrt{k_+k_2}$ fixed and allowing $\sqrt{k_+k_n}$ to vary across different Zn^{2+} concentrations, the primary nucleation rate, k_n, is the sole effective free parameter. Similarly, to check the effect on the elongation rate, k_+, as the effective free fitting parameter, $\sqrt{k_n/k_2}$ and $\sqrt{k_+k_2}$ were defined as global fit parameters. For this, the first term in Eq. **S9** was neglected as $\mathcal{O}\left(\frac{2k_+k_nm(0)^{n_c}}{n_c}\right) \ll \mathcal{O}(\text{other terms})$. When fitting $\sqrt{k_n/k_2}$ to one global value and allowing $\sqrt{k_+k_2}$ to vary, k_+ is the effective free fitting parameter.

Whereas a fit with k_n as the effective free fitting parameter resulted in an insufficient fit ($\chi^2 = 10.86$), the fits for k_2 and k_+ as free parameter describe equally well the aggregation kinetics with χ^2 values of 5.41 and 5.71 for k_2 and k_+ as free parameters, respectively (Fig. S4*A*). Both the relative elongation and secondary nucleation rate, where the other one is assumed to be unaffected, show about the same dependence on Zn^{2+} concentration (Fig. S4*B*). Thus, the effect of Zn^{2+} on $A\beta_{40}$ aggregation can be described by a change of k_2 and/or k_+. From this analysis it is, however, not possible to distinguish whether Zn^{2+} affects primarily k_2 or k_+ or both. The result from the global fit that the value of K_M did not significantly change in the presence of Zn^{2+} (Table S1) provides, however, evidence that primarily elongation reactions are inhibited by zinc. An unchanged K_M value indicates that both the attachment of peptides to the fibril surface and the formation and subsequent release of new aggregates are equally affected. The microscopic nature of these events is, however, fundamentally different and simultaneous inhibition of both processes seems less likely. To elucidated this issue in more detail preseeded experiments are performed that report on the effect on rate with which fibrils elongate (see the following section).

Preseeded Aggregation Kinetics

Seeded experiments can be used to distinguish whether primary or secondary nucleation events are primarily affected by Zn^{2+} (5). In addition, at high seed concentration the initial slope is proportional to the elongation rate and effects of Zn^{2+} on the elongation can be quantified (5).

Seeds were taken from samples that reached the final aggregation state characterized by either ThT end-point fluorescence (Fig. S2*A*) or CD signal (Fig. S2*B*). Seeds used for experiments displayed in Fig. S3 were produced by incubating a 10 μM $A\beta_{40}$ sample at 37 °C under continuous agitation (stirring by a small magnet). The aggregation process was monitored all of the time by recording the CD signal. The CD signal displayed a two-state transition from a mainly random coil-like signal at the start to a final β-structure (Fig. S2*B*). After about 5 h the transition was completed and the CD signal remained unchanged, which defined the final aggregation state (Fig. S2*B*). Alternatively, seeds used for Fig. S4*C*, *Right*, were taken from an aggregated sample (45 μM $A\beta_{40}$) that was incubated with 100 μM ThT at 37 °C in a 96-well plate under quiescent conditions and its sigmoidal ThT fluorescence signal increase was recorded (Fig. S2*A*). The aggregated samples were homogenized by drawing the solutions 10 or more times up and down through a 27-gauge syringe (inner diameter 0.21 mm) and subsequent sonication for 5 min. The aggregated and homogenized samples were then added to monomeric peptide as seeds. For very high seed concentrations (Fig. S4*C*, *Left*) monomeric peptide solutions at different Zn^{2+} concentrations were directly added to aggregated ThT end-point samples incubated with the same Zn^{2+} concentration, without any further treatment of the seeds.

Seeded kinetics experiments were performed under quiescent condition, first, for different $A\beta_{40}$ concentrations with Zn^{2+} added at $A\beta$:Zn^{2+} 10:1 molar equivalents and ∼1 μM seeds (Fig. S3*A*) and, second, at constant $A\beta_{40}$ concentration with different Zn^{2+} concentrations at two different seed:monomer ratios, 3 μM : 19 μM and 11.5 μM : 10 μM seed:monomer.

Aggregation traces of preseeded peptide at ∼1 μM seeds showed a sigmoidal behavior and reached the final state before a significant signal increase of the unseeded samples was observed (Fig. S3*A*). Variance weighted mean aggregation half times (of four replicates) were significantly prolonged in the presence of zinc at $A\beta$:Zn^{2+} 10:1 molar equivalents (Fig. S3*B*).

At large seed concentration new aggregates are generated predominately by adding monomeric peptide to fibril ends. The initial slope is, hence, proportional to the elongation rate (5). At very high seed concentration (11.5 μM : 10 μM seed:monomer) the aggregation behavior clearly exhibits a concave shape, that is, the seed concentration is above the critical seed concentration and the maximal growth rate is largest at the start (6). The initial slope was determined by a linear fit to first 18 and 30 min for 11.5 μM : 10 μM and 3 μM : 19 μM seed:monomer ratio, respectively, neglecting the very first time points due to temperature equilibration. Aggregation traces (averaged over three to five replicates) at different Zn^{2+} concentration yield a Zn^{2+}-dependent elongation rate (Fig. S4*C* and Fig. 2*D*). The relative elongation rate decreases with increasing Zn^{2+} concentration and shows about the same Zn^{2+} dependence for both seed:monomer ratios as was found from the global fit analysis of unseeded peptide (Fig. 2*D* and Fig. S4*C*, inset graphs).

NMR

^1H-^{15}N HSQC, ^{15}N CPMG relaxation dispersion, and diffusion experiments were acquired on a 700-MHz Bruker Avance spectrometer equipped with a cryogenic probe.

^{15}N CPMG relaxation rates were recorded of 75 μM ^{15}N-$A\beta_{40}$ with 20 μM Zn^{2+} for five different temperatures from 278 to 290 K in steps of 3 K (same sample) as well as with 10 μM Zn^{2+} and without Zn^{2+} (different samples) both at 281 K using a CPMG

pulse scheme (7) with a mixing time of 120 ms and 11 different delays between the 180° pulses as well as a reference experiment without the mixing period. To reduce any putative long-time-scale-event influences, relaxation dispersion data sampling was performed in an interleaved acquisition scheme meaning that slow aggregation affects all CPMG frequencies in the same manner. Relaxation rates were determined from cross-peak heights. These rates including data from five temperatures and two Zn^{2+} concentrations were fitted to a two-state chemical exchange model (8–10) as described in refs. 11 and 12. The calculated relaxation rates R_2^0 and the absolute chemical shift differences $|\Delta\delta|$ are residue-specific fitting parameters, whereas the population of the second state p_B and the chemical exchange rate k_{ex} are fitted as global parameters. $\Delta\delta$ was constrained to the same value for all temperatures and Zn^{2+} concentrations. Only residues with relaxation dispersion profiles featuring F-test values of $P < 0.03$ and 3-s^{-1} difference between the first and last point for 278–284 K were used for the fitting, which applied for eight residues. With 20 μM Zn^{2+} the first five (four) points of F4, R5, and S8 are close to the noise level and were therefore excluded from the fitting. To check the robustness of the fit including only the eight residues with significantly high relaxation dispersion amplitudes, a fit including all residues was also performed. This fit revealed essentially the same chemical shift changes for the eight high-amplitude profile residues and very small values for all other residues (Fig. 3*C*).

Diffusion experiments were performed at 281 K in D_2O on three different samples without and with 20 and 40 μM Zn^{2+} where the same small amount of water/Zn^{2+} solution (volume H_2O *ca.* 2%) was added to each sample. A list of 16 different gradient strengths with linear spacing, a gradient pulse length of 3 ms, and a diffusion time of 100 ms were applied for the diffusion measurements. Diffusion coefficients were determined using the integrated signals of the aromatic side chain protons. Errors were estimated from SD of five or more measurements (on the same sample). The hydrodynamic radius, R_H, was calculated from the translational diffusion coefficient, D_t, through the Stokes–Einstein equation, $R_H = k_B T/(6\pi\eta D_t)$, where k_B is the Boltzmann's constant and η the dynamic viscosity.

^{1}H-^{15}N HSQC cross-peaks in the presence of 15 mM LiDS were assigned using ref. 13 (determined at 298 K) and extrapolated to 281 K with a temperature scan in steps of 3 K.

Thermodynamics of Zn^{2+} Binding

Two-State Model for Zn^{2+} Binding. The temperature dependence of the Zn^{2+} bound state may be used to determine reaction-specific thermodynamic parameters. Assuming a 1:1 complex for the reaction product the Zn^{2+} binding process can be described by

$$A\beta_{40} + Zn^{2+} \underset{k_{off}}{\overset{k_{on}}{\rightleftharpoons}} A\beta_{40}Zn^{2+}.$$

The apparent dissociation constant K_D of this binding is given by the population of the bound state, p_B, and the initial Zn^{2+} and Aβ concentrations, $[Zn^{2+}]_0$ and $[A\beta]_0$:

$$K_D^{app} = \frac{(1-p_B)\cdot\left([Zn^{2+}]_0 - p_B[A\beta]_0\right)}{p_B}. \quad \text{[S11]}$$

The values of K_D^{app} at different temperatures are listed in Table 1.

Three-State Model for Zn^{2+} Binding. To describe folding of the N terminus around the Zn^{2+} ion as the rate-limiting step we applied a three-state model that includes Zn^{2+} binding to the peptide's N terminus and consequent folding of the N terminus:

$$A\beta_{40} + Zn^{2+} \underset{k_{off}}{\overset{k_{on}}{\rightleftharpoons}} A\beta_{40}Zn^{2+}(U) \underset{k_U}{\overset{k_F}{\rightleftharpoons}} A\beta_{40}Zn^{2+}(F).$$

The initial Zn^{2+} binding may be described by a dissociation constant $K_D = 6.6$ μM obtained from tyrosine fluorescence experiments using competitive titration with copper ions (14). The population of peptide that has a Zn^{2+} ion bound, p_{Zn}, may be calculated from the initial Aβ and Zn^{2+} concentrations, $[A\beta]_0$ and $[Zn^{2+}]_0$ and the dissociation constant by

$$p_{Zn} = \frac{\left([A\beta]_0 + [Zn^{2+}]_0 + K_D\right)}{2[A\beta]_0} - \frac{\sqrt{\left([A\beta]_0 + [Zn^{2+}]_0 + K_D\right)^2 - 4[A\beta]_0[Zn^{2+}]_0}}{2[A\beta]_0}. \quad \text{[S12]}$$

The fraction of peptides with a bound Zn^{2+} ion and the corresponding concentration are displayed in Table S2.

Gibbs Free Energy. The Gibbs free energy is calculated from the equilibrium constant, $K_{eq}^{U\to F}$, of the three-state model by

$$K_{eq}^{U\to F}(T) = \frac{p_F(T)}{p_U(T)} = \frac{p_B(T)}{p_{Zn} - p_B(T)} \quad \text{[S13]}$$

$$\Delta G^{U\to F}(T) = -RT \ln K_{eq}^{U\to F}(T), \quad \text{[S14]}$$

where the dissociation constant K_D and, hence, the Zn^{2+} bound population p_{Zn} are assumed to be temperature-independent and $p_F = p_B$ is the population of the folded state determined by relaxation dispersion measurements.

The simplest description for the Gibbs free energy is a linear dependence on temperature where ΔH^0 and ΔS^0 do not feature an explicit temperature dependence:

$$\Delta G(T) = \Delta H^0 - T\Delta S^0. \quad \text{[S15]}$$

To describe the curvature of the data points in Fig. 3*E* and Fig. S9 correctly a heat capacity is introduced describing an explicit temperature dependence of the enthalpy by $\Delta C_P = (\partial H/\partial T)_P$ (15):

$$\Delta G(T) = \Delta H_{T_m} - T\Delta S_{T_m} + \Delta C_P(T - T_m) - T\Delta C_P \ln(T/T_m), \quad \text{[S16]}$$

where the enthalpy and entropy are defined at a reference temperature, T_m. The temperature dependence of the enthalpy and entropy are given by

$$\Delta H(T) = \Delta H(T_m) + \Delta C_p(T - T_m) \quad \text{[S17]}$$

$$\Delta S(T) = \Delta S(T_m) + \Delta C_p \ln(T/T_m). \quad \text{[S18]}$$

We chose the reference temperature as a melting temperature by $T_m = \Delta H^0/\Delta S^0$ where ΔH^0 and ΔS^0 are determined from a linear fit at higher temperatures. The explicit temperature dependence of $\Delta H(T)$ and $\Delta S(T)$ is displayed in Fig. S9. To test the impact of the previously determined $K_D = 6.6$ μM (14) we calculated $\Delta G(T)$ assuming an uncertainty of 5 K_D and $K_D/5$ (Fig. S9). We found that the absolute values of $\Delta G(T)$ are shifted whereas the overall behavior is conserved.

Estimation of Population of Folded State from Diffusion Data

The measured translational diffusion coefficient, D_{obs}, is given as the population weighted average of the diffusion coefficients of Zn^{2+}-bound folded peptide, D_B, and the nonfolded population

(including free and Zn^{2+}-bound unfolded peptides), D_{nF}, with $D_{nF} \approx D_{free}$:

$$D_{obs} = (1 - p_B) \cdot D_{free} + p_B \cdot D_B. \quad \textbf{[S19]}$$

Using the population of the bound state as determined by relaxation dispersion measurements in the presence of 20 μM Zn^{2+} the diffusion coefficient of the folded state can be determined, when assuming the same diffusion coefficient of the bound state, D_B, at 20 and 40 μM Zn^{2+}. The bound population in the presence of 40 μM Zn^{2+} is thereby given by

$$p_{B,40\mu M} = \frac{D_{obs,40\mu M} - D_{free}}{D_B - D_{free}} = 12.6\%. \quad \textbf{[S20]}$$

This estimate indicates that the population of folded peptide increases linearly with increasing Zn^{2+} concentration (Fig. S8). With Eq. **S11** the apparent dissociation constant can be estimated to ~210 μM.

1. Abelein A, Bolognesi B, Dobson CM, Gräslund A, Lendel C (2012) Hydrophobicity and conformational change as mechanistic determinants for nonspecific modulators of amyloid β self-assembly. *Biochemistry* 51(1):126–137.
2. Meisl G, et al. (2014) Differences in nucleation behavior underlie the contrasting aggregation kinetics of the Aβ40 and Aβ42 peptides. *Proc Natl Acad Sci USA* 111(26):9384–9389.
3. Cohen SIA, et al. (2013) Proliferation of amyloid-β42 aggregates occurs through a secondary nucleation mechanism. *Proc Natl Acad Sci USA* 110(24):9758–9763.
4. Barth A (2007) Infrared spectroscopy of proteins. *Biochim Biophys Acta* 1767(9):1073–1101.
5. Cohen SIA, Vendruscolo M, Dobson CM, Knowles TPJ (2012) From macroscopic measurements to microscopic mechanisms of protein aggregation. *J Mol Biol* 421(2-3):160–171.
6. Cohen SIA, et al. (2011) Nucleated polymerization with secondary pathways. I. Time evolution of the principal moments. *J Chem Phys* 135(6):065105.
7. Tollinger M, Skrynnikov NR, Mulder FA, Forman-Kay JD, Kay LE (2001) Slow dynamics in folded and unfolded states of an SH3 domain. *J Am Chem Soc* 123(46): 11341–11352.
8. Palmer AG, 3rd, Kroenke CD, Loria JP (2001) Nuclear magnetic resonance methods for quantifying microsecond-to-millisecond motions in biological macromolecules. *Methods Enzymol* 339:204–238.
9. Carver J, Richards R (1972) A general two-site solution for the chemical exchange produced dependence of T_2 upon the Carr-Purcell pulse separation. *J Magn Reson* 6(1):89–105.
10. Davis DG, Perlman ME, London RE (1994) Direct measurements of the dissociation-rate constant for inhibitor-enzyme complexes via the T1 rho and T2 (CPMG) methods. *J Magn Reson B* 104(3):266–275.
11. Abelein A, Lang L, Lendel C, Gräslund A, Danielsson J (2012) Transient small molecule interactions kinetically modulate amyloid β peptide self-assembly. *FEBS Lett* 586(22): 3991–3995.
12. Abelein A, et al. (2013) Formation of dynamic soluble surfactant-induced amyloid β peptide aggregation intermediates. *J Biol Chem* 288(32):23518–23528.
13. Jarvet J, Danielsson J, Damberg P, Oleszczuk M, Gräslund A (2007) Positioning of the Alzheimer Abeta(1-40) peptide in SDS micelles using NMR and paramagnetic probes. *J Biomol NMR* 39(1):63–72.
14. Danielsson J, Pierattelli R, Banci L, Gräslund A (2007) High-resolution NMR studies of the zinc-binding site of the Alzheimer's amyloid beta-peptide. *FEBS J* 274(1):46–59.
15. Oliveberg M, Tan YJ, Fersht AR (1995) Negative activation enthalpies in the kinetics of protein folding. *Proc Natl Acad Sci USA* 92(19):8926–8929.

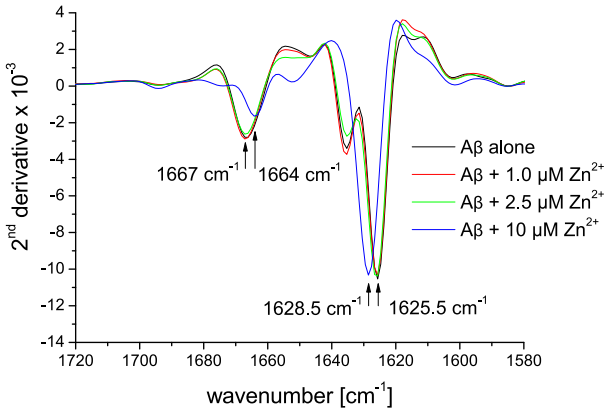

Fig. S1. ATR-Infrared spectra of aged $A\beta_{40}$ samples incubated at different Zn^{2+} concentrations and recorded as dried films. The films were obtained from precipitates (after 20 min of centrifugation) of ThT fluorescence end-point samples. The second derivative of the IR absorbance is displayed and the curves are normalized to same intensity of the minimum at 1,625–1,629 cm^{-1}. For $A\beta_{40}$ alone and in the presence of low zinc concentrations (≤2.5 μM) the spectra are almost identical, indicating a similar morphology of the fibril structures. In contrast, at 10 μM Zn^{2+} the IR spectrum is clearly different, suggesting the formation of different fibril morphologies under these conditions.

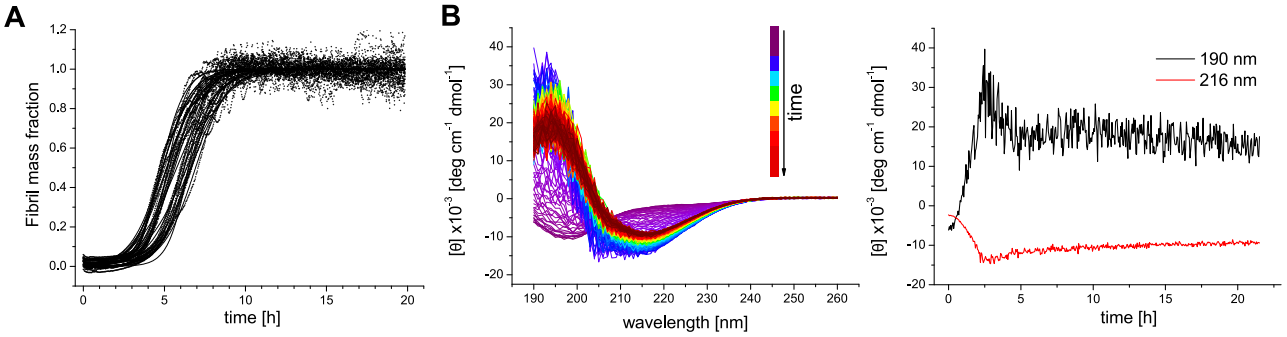

Fig. S2. Aggregation kinetics of samples whose final states were used for seeding experiments. (*A*) ThT fluorescence of 45 μM $A\beta_{40}$ was monitored at at 37 °C and under quiescent conditions. (*B*) Far-UV CD kinetics of 10 μM Aβ recorded at 37 °C and continuous stirring. The spectrum shows a transition from random coil-like at the start to a final state that exhibited a β-structure.

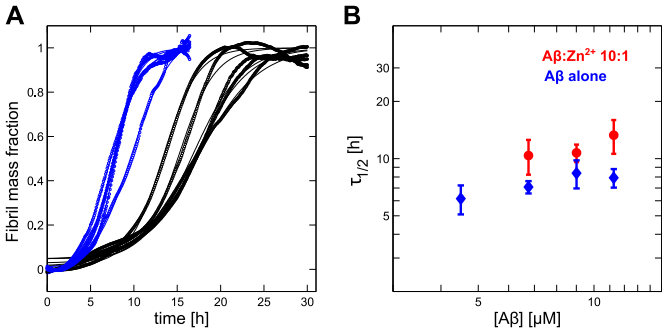

Fig. S3. (*A*) Aggregation kinetics under quiescent conditions of 10 μM Aβ (black) and 11.3 μM Aβ with 1 μM seeds (blue). The intensity was normalized to the same final signal. (*B*) Fitted $\tau_{1/2}$ values (from sigmoidal fits) under quiescent conditions for seeded Aβ samples without (blue) and with (red) Zn^{2+} at at molar equivalents of $A\beta_{40}$:Zn^{2+} 10:1.

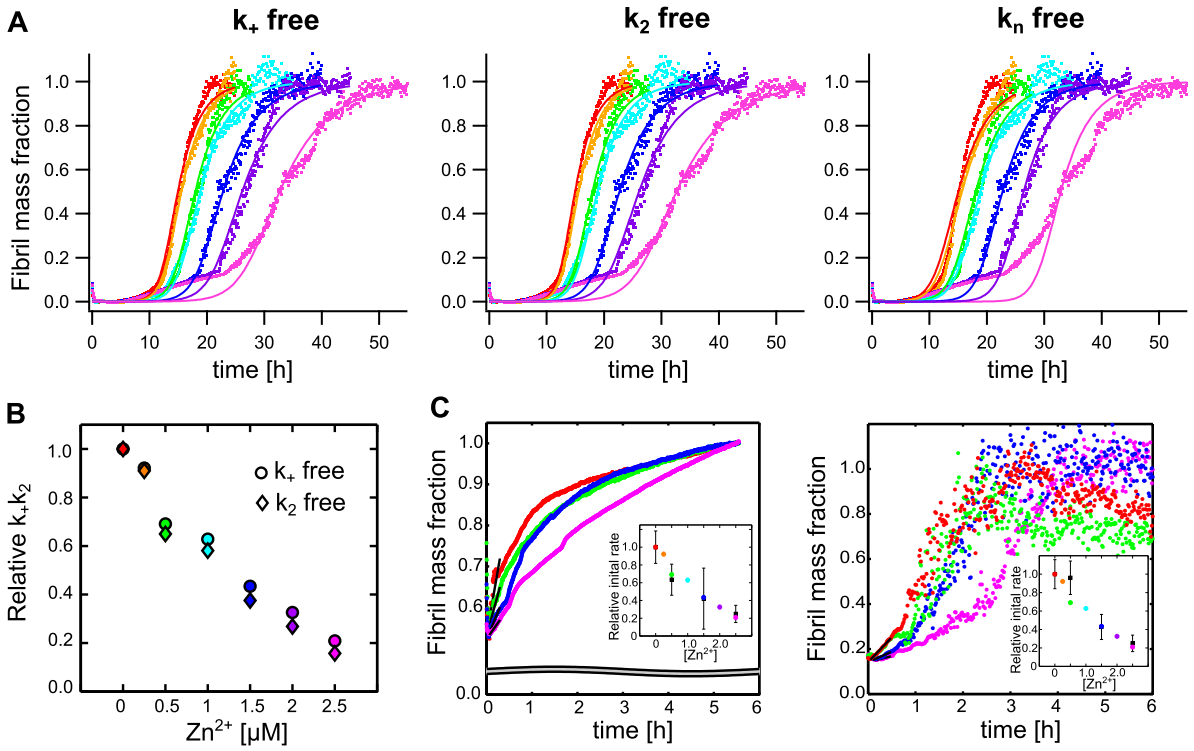

Fig. S4. (*A*) Global fit analysis of 20 μM $A\beta_{40}$ in the presence of 0–2.5 μM Zn^{2+} where either k_n, k_2, or k_+ is the effective free fitting parameter. The χ^2 values for the different fits are 10.86 (k_n free), 5.41 (k_2 free), and 5.71 (k_+ free). The color code used is 0 (red), 0.25 (orange), 0.5 (green), 1 (cyan), 1.5 (blue), 2 (violet), and 2.5 (pink) μM Zn^{2+}. (*B*) Relative global fit parameter (squared), k_+k_2, where one microscopic rate is the effective free fitting parameter and the other one is effectively constant. (*C*) Preformed fibrils were added to monomeric $A\beta_{40}$ at different Zn^{2+} concentrations and where the initial slope (black line) was fitted to averaged aggregation traces. The experiment was performed at 11.5 μM seeds to 10 μM monomers (*Left*), and 3 μM seeds to 19 μM monomers (*Right*). The inserted graphs display the initial rates compared with the relative elongation rates obtained from the global fit analysis.

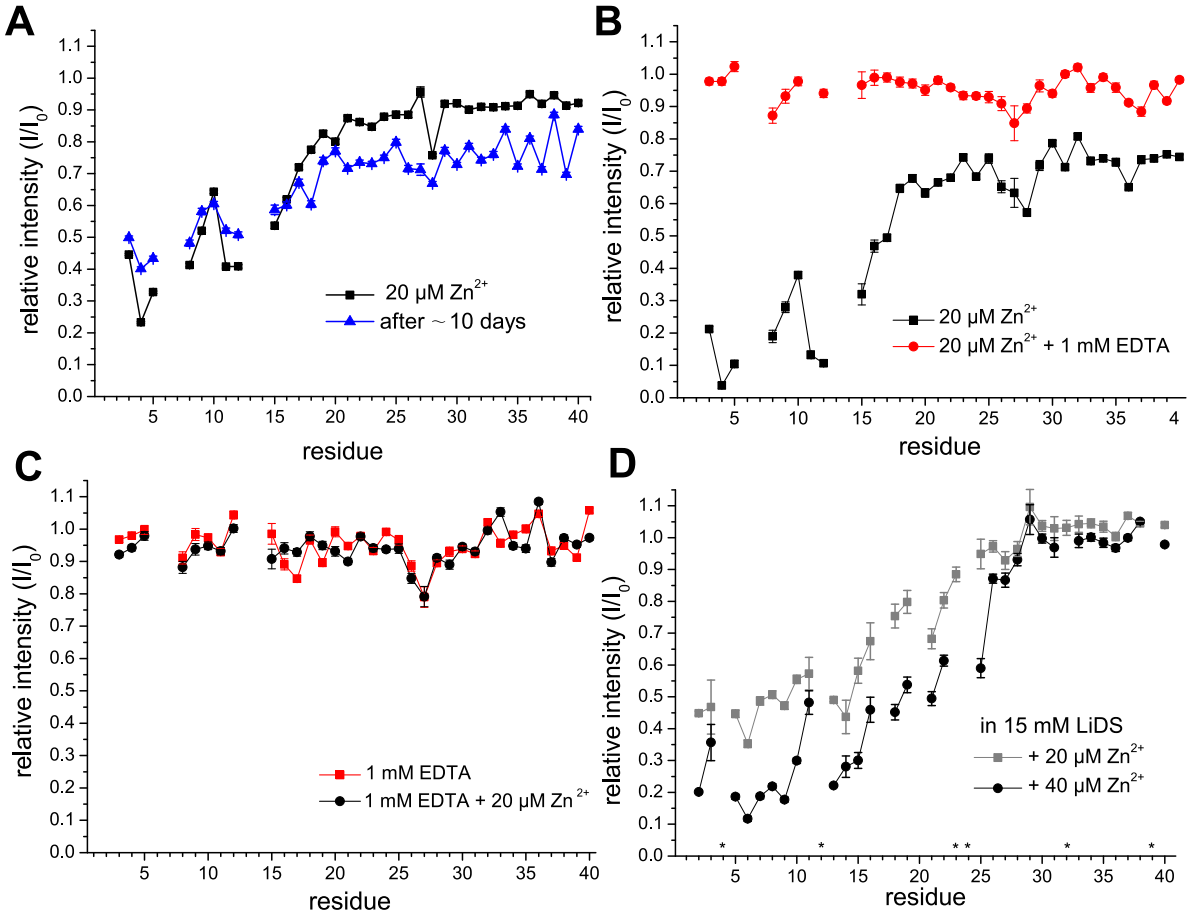

Fig. S5. (*A*) Relative ^{1}H-^{15}N HSQC cross-peak intensity of 75 μM $A\beta_{40}$ in 10 mM Hepes buffer, pH 7.4, at 278 K upon addition of 20 μM $ZnCl_2$ before (black) and after the relaxation dispersion measurements at different temperatures (278–290 K) performed in ~10 d. (*B* and *C*) Relative ^{1}H-^{15}N HSQC cross-peak intensity of 75 μM $A\beta_{40}$ in 10 mM Hepes buffer, pH 7.2, at 281 K upon addition of 20 μM Zn^{2+} followed by 1 mM EDTA (*B*) and in reverse order (*C*) showing the reversible signal intensity loss in the N-terminal part of the peptide. The small signal loss in the C terminus may be assigned to formation of small amounts of aggregates. The histidine mediated zinc coordination is highly pH-dependent, and at pH 5.3 virtually no binding is observed (1). (*D*) Relative ^{1}H-^{15}N HSQC cross-peak intensities of 75 μM Aβ in 10 mM Hepes buffer, pH 7.1, with 15 mM LiDS at 281 K upon addition of 20 (light gray) and 40 μM Zn^{2+} (black). Residues marked with a star showed overlap with other residues and were excluded from the analysis. Error bars display the signal-to-noise ratio.

1. Ghalebani L, Wahlström A, Danielsson J, Wärmländer SKTS, Gräslund A (2012) pH-dependence of the specific binding of Cu(II) and Zn(II) ions to the amyloid-β peptide. *Biochem Biophys Res Commun* 421(3):554–560.

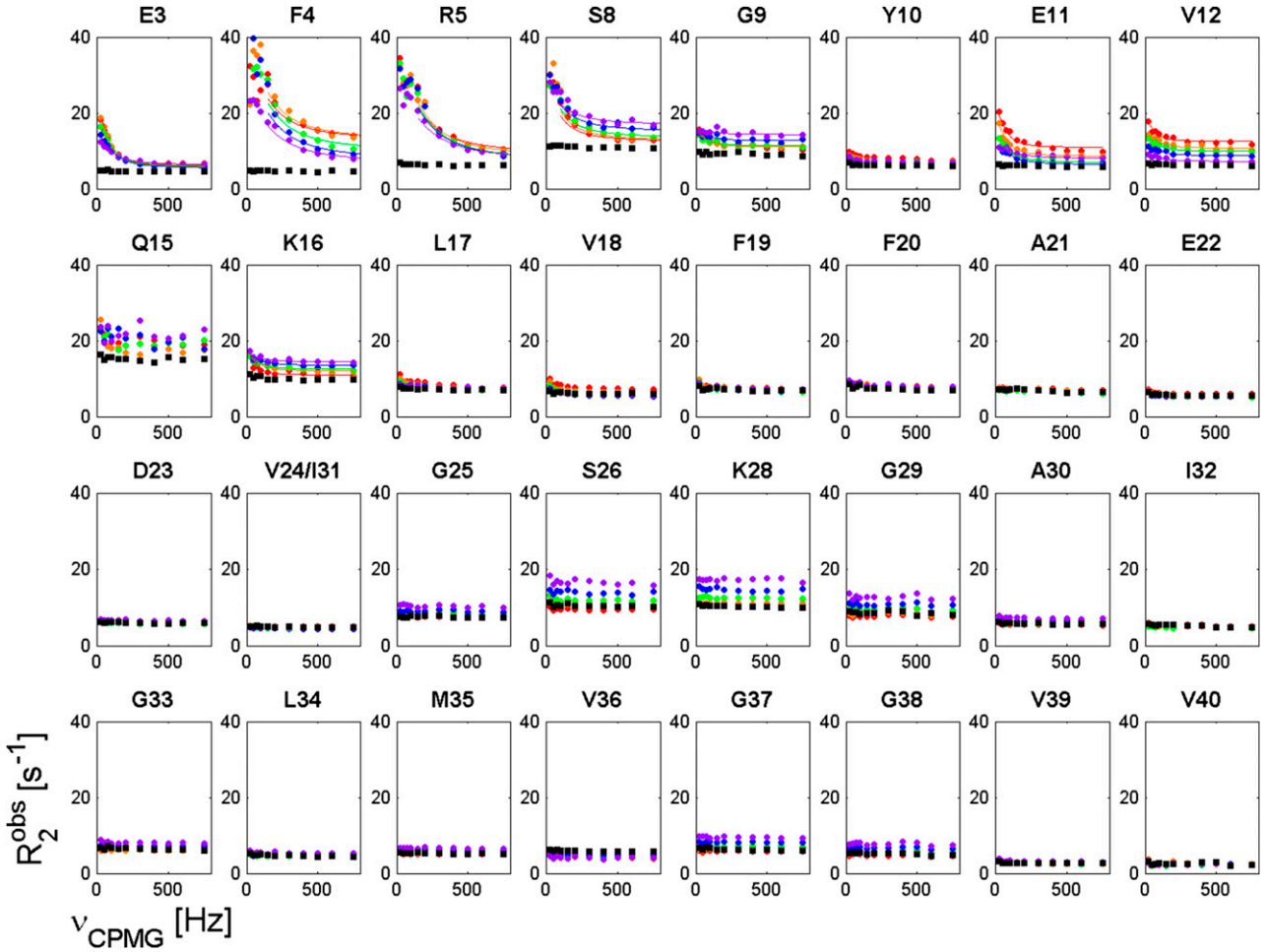

Fig. S6. Relaxation dispersion profiles for Aβ in the presence of 20 μM Zn^{2+} (circles) at 278 (red), 281 (orange), 284 (green), 287 (blue), and 290 K (violet) and Aβ alone at 281 K (black squares). The global fit routine included data from eight residues with significant relaxation dispersion amplitudes at five temperatures with two Zn^{2+} concentrations at 281 K.

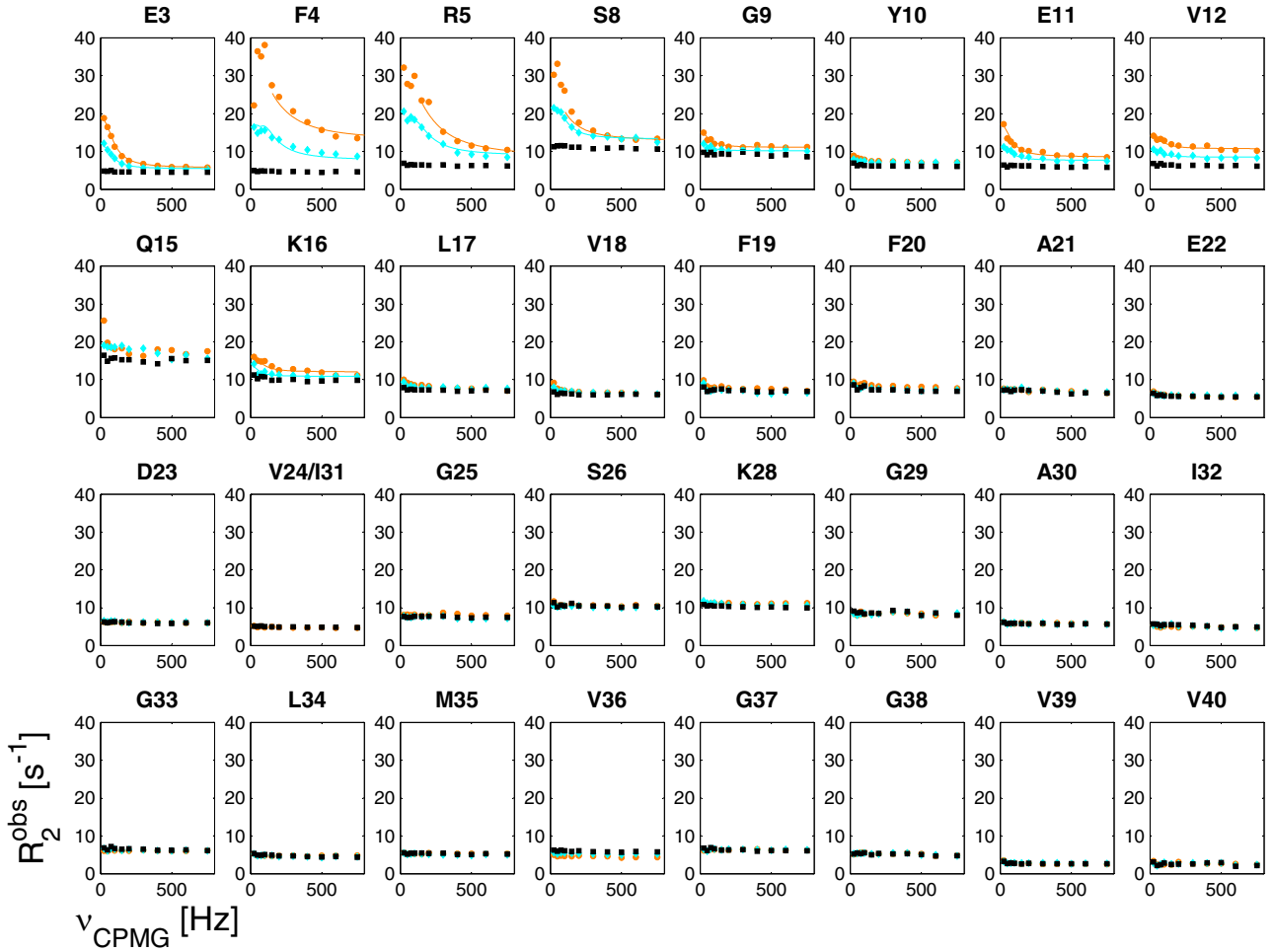

Fig. S7. Relaxation dispersion profiles for Aβ in the presence of 10 (diamonds, cyan) and 20 μM Zn^{2+} (circles, orange) as well as Aβ alone (black squares) at 281 K. The global fit routine included data from eight residues with significant relaxation dispersion amplitudes at five temperatures with two Zn^{2+} concentrations at 281 K.

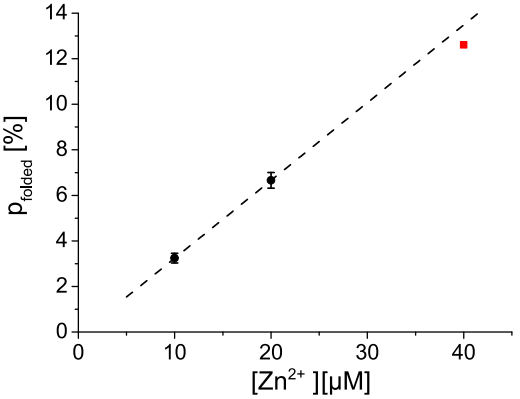

Fig. S8. Concentration dependence of the folded state on Zn^{2+} concentration. The data points for 10 and 20 μM were calculated as presented in Table 1. The value for 40 μM Zn^{2+} was estimated from diffusion data.

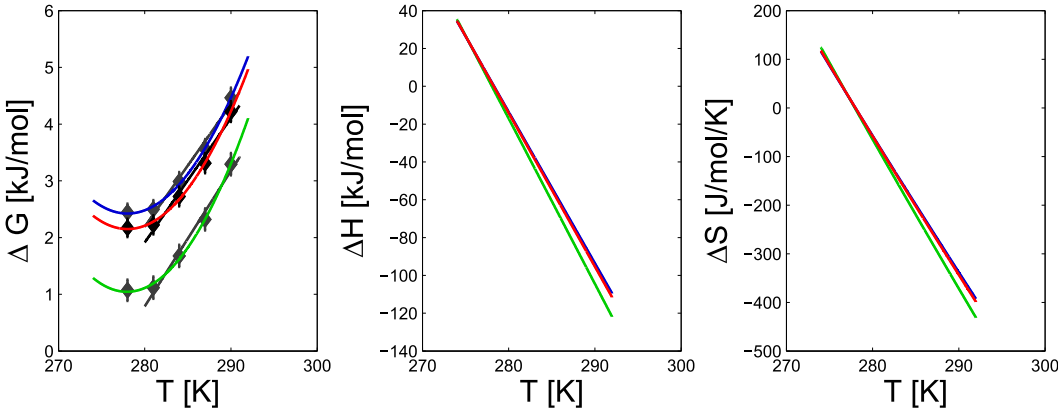

Fig. S9. Estimation of error impact of K_D on thermodynamic parameters. A uncertainty factor of 5 was assumed, that is, $5K_D$ (green) and $K_D/5$ (blue). The thermodynamic parameters were calculated according to Eqs. **S16**, **S17**, and **S18**.

Table S1. Global fit parameters for $A\beta_{40}$ alone and in the presence of Zn^{2+} at $A\beta$:Zn^{2+} 10:1 molar equivalents were obtained using Eq. S1

Fitting parameter	Aβ alone	Aβ:Zn^{2+} 10:1
$\sqrt{k_n k_+}$, $M^{-1}\cdot s^{-1}$	$2.3 \pm 0.3 \cdot 10^{-2}$	$0.98 \pm 0.08 \cdot 10^{-2}$
$\sqrt{k_+ k_2}$, $M^{-3/2}\cdot s^{-1}$	$3.85 \cdot 10^3$*	$2.15 \cdot 10^3$*
$\sqrt{K_M}$, μM	14.5 ± 2.6	11.6 ± 0.6
$m(0)$ Aβ alone,† μM	10.6 ± 0.3; 11.1 ± 0.4; 13.4 ± 0.6; 15.8 ± 1.0; 17.5 ± 1.3; 19.0 ± 1.6	
$m(0)$ Aβ + Zn^{2+},† μM	10.3 ± 0.1; 11.0 ± 0.1; 14.5 ± 0.3; 17.0 ± 0.4; 18.1 ± 0.5; 19.0 ± 0.5	

Errors are displayed as fitting errors, which report on the quality of the fit, whereas experimental errors may be substantially larger.
*Fitting error $< 2 \cdot 10^{-1} \cdot M^{-3/2} \cdot s^{-1}$.
†Constrained to ±1 μM of experimentally determined monomer concentration.

Table S2. Estimation of Zn^{2+} bound population from fluorescence titration experiments using Eq. S12 with a total peptide concentration of 75 μM

Amount zinc-bound peptide	20 μM Zn^{2+}	10 μM Zn^{2+}
p_{Zn}, %	24	12
$[A\beta]_{bound}$, μM	17.9	9.1